Semnan University

Journal of Heat and Mass Transfer Research

Journal homepage: https://jhmtr.semnan.ac.ir

ISSN: 2383-3068

Research Article

Magnetic Field Effects on Convective Heat Transfer of Ferrofluid from a Heated Sphere in Porous Media

Ayesha Aktar [a], Sharaban Thohura [a], Md. Mamun Molla [b,c]*

[a] *Department of Mathematics, Jagannath University, Dhaka-1100, Bangladesh*

[b] *Department of Mathematics & Physics, North South University (NSU), Dhaka-1229, Bangladesh*

[c] *Center for Applied and Computational Sciences (CACS), NSU, Dhaka-1229, Bangladesh*

ARTICLE INFO

Article history:

Received: 2024-04-19

Revised: 2024-11-09

Accepted: 2024-11-29

Keywords:

Magnetohydrodynamic;
Ferrofluid;
Heated sphere;
Porous media;
Heat transfer;
Finite difference method.

ABSTRACT

The impact of a magnetic field on the convective heat transfer of ferrofluids from a heated sphere immersed in a porous medium is investigated. The dimensional governing boundary layer equations are initially transformed into a convenient non-dimensional form utilizing the non-dimensional variables. The resulting nonlinear systems of equations are then numerically solved inside the computing domain into a regular rectangle using the effective Finite Difference Method (FDM). Numerical outcomes are then represented in terms of local Nusselt number, velocity, temperature profile, and skin friction coefficient, respectively for a range of porosity parameters, ϵ = 0.4, 0.6, 0.8, magnetic effect parameter or Hartmann number, Ha = 0.0, 1.0, 3.0, 5.0 and the ferroparticle volume fraction coefficients, ϕ = 0%, 2%, 4%, 6%. It is thought that the base fluid's Prandtl number, $Pr = 6.8733$, is constant. In addition, the flow pattern inside the boundary layer region is shown using streamlines and isotherms, and the underlying physics of the flow behavior is then explored. There is a graphical presentation of the data. The findings show that velocity decreases with increasing value Ha, ϕ and ϵ. An increase in the Hartmann number Ha causes the temperature to rise. The local N_u and C_f are decreasing as Ha and ϕ values increase. With an increase in the porosity parameter ϵ and ϕ, the temperature profile rises and the C_f and local N_u decrease. For increasing Ha, the figure of streamlines seems to depict functions with more gradual changes, and for isotherms, it represents functions with sharper, exponential-like increases. While many works focus on ferrofluids or porous media individually, combining the study of heat transfer in ferrofluids within porous structures can represent a distinct focus. The problem is crucial for developing advanced heat transfer technologies for more efficient energy management in various engineering applications.

1. Introduction

MHD is the study of electrically conductive fluids' motion and magnetic properties, also known as magneto-fluid dynamics or hydro-magnetics [1]. MHD has applications in a wide range of physical domains, encompassing cosmic plasmas and liquid metals. Aerodynamics heating, petroleum industry, geophysics, MHD power generators, plasma physics, fluid droplet sprays, MHD pumps, electrostatic precipitation, and sulfur cleaning of crude oil are a few examples of these domains [2–4]. Hannes Alfvén won the Nobel Award in 1970 in Physics for his invention of the field of magneto-hydrodynamics. The essential principle of MHD states that

* **Corresponding author.**
E-mail address: *mamun.molla@northsouth.edu*

Cite this article as:

Aktar, A., Thohura, S. and Molla, M. M., 2025. Magnetic Field Effects on Convective Heat Transfer of Ferrofluid from a Heated Sphere in Porous Media. *Journal of Heat and Mass Transfer Research*, 12(1), pp. 177-192.

https://doi.org/10.22075/JHMTR.2024.33841.1554

currents in flowing conductive fluids can be generated by magnetic fields and that these currents polarize the fluid and alter the field of magnetic attraction in the opposite orientation.

Using the Lattice Boltzmann Technique, Sheikholeslami et al. [5] examine MHD flow using a Cu water nanofluid in a concentric annulus. The statistics show that the enhance- ment ratio increases with decreasing Raylei- gh number and increases with increasing Hartmann number. Additionally, a direct cor- relation between the Nusselt number and the nanoparticle volume fraction and an inverse relationship with the Hartmann number may be deduced. Ellahi et al. [6] have examined the MHD motion of a non-Newtonian nanofluid via a conduit. It is observed that the MHD factor diminishes fluid motion even in the presence of different viscosities and that the pattern of velocity is greater than the temperature curve. The features of heat transfer in a heat pipe with an ionic magnetic fluid (MF) maintained by ionized citrate (JC-1) as the working fluid are covered by Nakatsuka et al. [7] as well as actual visual observation of boiled aquatic and ionic MFs is also covered. Finally, the citrateion stabilized MF performed as expected, was stable, and at elevated temperatures, produced no non-condensed gas. This kind of magnetic fluid is thought to be the perfect operating liquid for applicatio- ns involving heat transfer. Poddar et al. [8] have examined the mass transfer of heat from thermally radiated and dissipative fluids via (MHD) boundary layer (BL) over an infinite plate oriented vertically, taking into account thermal diffusion and generated magnetic fields. According to the results, the induced magnetic field decreased as the magnetic factor's estimation increased.

Among the three essential methods of heat transfer is convection. Mass transfer is involved in this thermal exchange phenomenon. When convection is generated by external mechanical devices, like fans or pumps, it is said to be forced convection. It is known as natural or free convection when it occurs on its own [9]. Because of their low usage of energy, simplicity, and ease of maintenance, natural convection systems are particularly favorable in various sectors and engineering settings [10]. For instance, nuclear reactors [11, 12], food industries [13, 14], power stations [15, 16], solar collectors, building ventilation, and electronic package cooling. Only under the influence of a gravitational field or another appropriate acceleration, such as centrifugal force, acceleration, or Coriolis force, is free convection conceivable. Sekhar et al. [17] have investigated how the fluctuating temperature and mass transport cause the unstable MHD convection to flow during loosely packed porous media into a precipita- tely beginning perpendicular plate. It is found that increasing the penetrability parameter's quantities increases the velocity's magnitude. By increasing the radiating parameter, the velocity's magnitude is increased as it continuously trims down. With time, the velocity rises. A rise in the Prandtl number reduces the velocity's magnitude. An increase in the radiating parameters and/or Prandtl numbers lowers the temperature. The concentration profile's entire liquid area resulted from the Schmidt number's increasing quantities. As the radiating parameter and Prandtl number increase, the Nusselt number also increases. Hamma et al. [18] investigated the effects of a magnetic field on thermosolute natural convection in porous, isotropic, and saturated media containing Casson nano fluids (aluminum nanoparticles) using both theoretical and numerical modeling. As the Casson fluid parameter increases, heat and mass transmission increase as well; this increase is considerable for the case of β between 0.1 and 0.4. Additionally, it rises in tandem with the number of thrust ratios, thermal conductivity ratios, and thermal Rayleigh numbers. When the thermal Rayleigh number falls below the threshold, the latter does not change. In the opposite, we observe that as the Hartmann Soret and Dufour numbers rise, the thermosolutal transfer decreases unevenly. The findings of a numerical study on heat transfer by free convection within a slanted enclosure holding a water-CuO nano fluid were investigated by Ghasemi et al. [19]. The results demonstrate that Heat transmission is enhanced when pure water is mixed with nanoparticles. Nonetheless, the heat transmission rate can be raised by an ideal rigid volume fraction. The findings also demonstrate that, for large Rayleigh numbers, the angle of inclination significantly affects both the flow and temperature domains as well as the efficiency of heat transmission. Analysis of numerical and qualitative research on fluid flow and heat sinks with naturally occurring convective heat transfer has revealed that, in reality, depending on the Rayleigh number and rigid volume fraction, a certain inclination angle maximizes the heat transmission rate.

Liquids that react to magnetic fields are known as ferrofluids. In a liquid medium, they are magnetic material colloidal suspens- ions. Ferromagnetic nanoparticles, usually made of metallic alloys or transition metal oxides, are suspended in a carrier fluid to form ferromagnetic nanofluids, a type of nanocomposites [20]. Because of its essential properties, which include the ability to levitate both magnetic and non-magnetic materials, ferro -fluids are exploited in engineering applications

[21–25]. Ferrofluids have been widely used in industrial applications such as medication delivery, heat transfer, functional materials, biosensors, and 3D printing since their rapid development [26]. Applying the Finite Element Method based on Control Volume, the numerical modeling of Fe_3O_4-water nanofluid mixed convection heat transmission in a lid-driven semi-annulus beneath an irregular electromagnetic field was studied by Sheikholeslami et al. [27]. The outcomes demonstrate that nanoparticle volume fraction and the Nusselt number have an immediate correlation, but magnetic numbers, the Hartmann, and the Nusselt number have a reverse relationship. It is also discovered that when the viscosity based on the magnetic field is taken into account, the Nusselt number increases. The effects of a magnet field outside the system on the thermophysical properties of a ferrofluid were studied by Alsaady et al. [28]. The findings show that a ferrofluid can have 300 times the ability to conduct heat of a base fluid. Moreover, the creation of chains-like particle assemblies regarding the temperature gradient in the magnetic field can cause a fluid's viscosity to increase. The contribution of Fe_3O_4 to enhanced heat transmission in an axisymmetric fluid across a disk that revolves was studied by Farooq et al. [29]. It is discovered that the radial velocity drops, and the tangential motion of the flow becomes stronger as the volumetric concentration of nanoparticles increases.

Solid materials with pore features are known as porous media. Especially in the case of natural systems like rock and soil, porous media comprise a vast class of complex systems [30]. The heat transfer in an enclosed porous cavity made of water-based ferrofluid that is connected to a new permeable (suction/injection) chamber is investigated by Siddiqui et al. [31]. It is found that increasing either (i) the ferroparticle concentration or (ii) the Lorentz force results in an increase in the Nusselt number at the left wall but a decrease at the right wall. However, the way that the Kelvin force and the Lorentz force affect the Nusselt number differs in that the former causes the Nusselt number to decrease at the left wall while the latter, or its counterpart, the Hartmann number, inten- sifies near the right wall. Furthermore, if the Hartmann number climbs from 0 to 50, the Nusselt number at the cavity's left wall increases by almost 1.4 times. The study of flow in porous media is relevant to numerous engineering disciplines, such as chemical, water, mechanical, civil, and environmental engineering [32]. Using 2D models to invest in 3D flows' properties in porous media by Marafini et al. [33], Because through porous media, two dimensional and three dimensional flows differ significantly, the results of pore scale simulation show that using the two-dimensional methods frequently results in conflicting. The theoretical and practical aspects of the DDIF approach for characterizing pore geometry in porous media were examined by Song [34]. In the first part, the internal field, its origin, and the statistical characteristics of its spatial inhomogeneity were covered. The important thing is that the internal field is statistically identical in different pores and shows fluctuation inside a single hole. The process for obtaining the pore size distribution was reviewed in the second section, along with the pulse sequences, spectral characteristics, and echo shapes. Understanding the diffusion dyna mics in porous media theoretically was the focus of the final portion. It demonstrates how effect tively the eigenmode formalism works for DDIF experiment analysis and how it can be directly interpreted in terms of the pore geometry characteristics. Sakthivel et al. [35] examined the problem of axisymmetric, duo stress fluid continuously creeping past a permeable sphere encircled by a rigid core. The results show that the existence of stress jump coefficients reduces the couple stresses, pressure, and drag force of the consistent flow of a couple stress flow past a permeable sphere surrounded by a rigid core with stress skip condition. This is in contrast to the flow of a pair stress fluid through a permeable sphere in an ongoing shear stress scenario.

The aim of this work is to study the free convection boundary layer flow across a sphere in the presence of a field of magnets. Beg et al. [36] demonstrated the theoretical and numerical aspects of magnetohydrodyn- amic free convection from a sphere contained in an electrically conducting fluid-saturated porous regime with heat generation. According to the results, a higher Darcy number causes the flow to accelerate (i.e., increase velocity) while lowering the fluid's temperature. While increasing the magnetic field (Nm) raises the temperature, it decreases velocity. When a heat source ($H > 0$) generates heat, temperature and velocity rise, and the opposite is true for heat sinks ($H < 0$), which absorb heat. Both velocity and surface shear stress decrease as the inertial porous drag parameter, Fs, increases. Both velocity and the surface temperature gradient are reduced when the free convection parameter, Gr, is increased.

In light of the foregoing discussion, it is clear that a great deal of studies have been done on magnetohydrodynamics free convection flow correspondingly a variety of surfaces while taking different boundary conditions. But most of them deal with a Newtonian fluid or a flat surface. Flat surfaces and irregular surfaces do not pique the scientific community's curiosity too much

because uneven surface geometry occurs in most real-world scenarios. It is important to emphasize the role that ferrofluid plays in the process of heat transmission as well. To the utmost of the writers' understanding, no literature has been released on the topic of the current investigation and the study of heat transmission in ferrofluids within porous structures can represent a discrete topic, even though many works concentrate on ferrofluids or porous media separately. This adds complexity and could reveal occurrences that haven't been thoroughly investigated in earlier studies. As a result, the results of this study are distinct, and it is expected that they will be helpful for subsequent research on the analysis of heat transmission properties within the ferrofluid boundary layer flow. Since conventional heat management methods (altering temperature or flow rates) are less dynamic and challenge- ing to swiftly or remotely adjust, controlling heat transfer with a magnetic field is a novel approach. In systems where efficient heat transfer or dissipation is required, the complex but creative interaction of ferrofluid with porous media under a magnetic field can improve heat transfer efficiency. Significant cooling system applications could come from this research, especially for electronics, reactors, or systems where conventional coolants are less efficient. The application of magnetic fields to modify fluid flow and heat transfer provides a non-invasive, adjustable method that is difficult to do with traditional fluids. It may result in advancements in heat exchangers with intricate shapes used in biomedicine, where localized heating can be necessary for focused medication adminis tration. This study may close a knowledge gap regarding the effects of magnetic fields on ferrofluid heat transfer and their behavior in porous media. The findings may aid in the creation of new simulations and models for performance prediction and optimization, bringing about advancements in thermal management systems and improving techno logies that depend on accurate heat control.

Table 1 provides a comparsion between the current study and the similar studies available in the literature.

Table 1. A comparsion between the current study and the similar studies available in the literature

Study	Key Findings	Methodology	Research Gaps Addressed	Novel Contribution of our work
Poddar et al.[8]	Thermal radiation and viscous dissipation significantly impact temperature and velocity profiles in the fluid under MHD conditions."	using finite difference methods, specifically using the Keller-box scheme.	Lacks specificity on ferrofluids, effects in porous media, and convective heat transfer around spherical geometries.	more specialized investigation relevant to ferrofluid behavior and heat transfer applications in porous structures.
Song et al.[34]	The study shows that magnetic resonance can identify pore sizes by analyzing water molecule movement and relaxation rates.	The study uses NMR to measure T_1 and T_2 relaxation times of fluids in porous media, linking these times to pore size through molecular interactions with pore surfaces.	It innovates by using magnetic resonance to study pore structure only.	The ferrofluid study reveals new insights into how magnetic fields influence convective heat transfer in porous environments.

2. Formulation of the Problem

2.1. Physical Properties of Ferrofluid

The thermophysical characteristics of solid ferroparticles (Fe_3O_4) and the foundational fluid (H_2O) are quantitatively displayed in Table 2 [37–41].

Xuan and Li [42] and Ghanbarpour et al. [43] have proposed the mixture rule, which is used to calculate the ferrofluid's effective density (ρ_{ff}):

$$\rho_{ff} = (1-\phi)\rho_f + \phi\rho_s \quad (1)$$

where ρ_s is the density of the solid particles, ρ_f is the density of the base fluid, and ϕ is the volume fraction of the ferro-particles.

Table 2. Thermophysical properties of base fluid and solid ferroparticles

Physical Properties	Ferro-particles (Fe_3O_4)	Base-fluid (H_2O)
C_p [J kg^{-1} K^{-1}]	670	4179
ρ [kg m^{-3}]	5200	997.1
K [W m^{-1} K^{-1}]	6	0.613
$\beta \times 10^{-5}$ [K^{-1}]	1.18	20.7
σ [S m^{-1}]	25000	0.05
μ [kg m^{-1} s^{-1}]		0.001003
Pr		6.8377

The heat capacity $(\rho C_\rho)_{ff}$ of the ferrofluid and the thermal expansion coefficient $(\rho\beta)_{ff}$ determined from [43] are as follows:

$$(\rho C_\rho)_{ff} = (\rho C_\rho)_f (1-\phi) + (\rho C_\rho)_s \phi \quad (2)$$

$$(\rho\beta)_{ff} = (\rho\beta)_f (1-\phi) + (\rho\beta)_s \phi \quad (3)$$

The electrical conductivity σ_{ff} of the ferrofluid and the effective thermal conductivity k_{ff} can be approximated by [44,45] as:

$$k_{ff} = k_f \frac{k_s + 2k_f + 2\phi(k_f - k_s)}{k_s + 2k_f - \phi(k_f - k_s)} \quad (4)$$

$$\sigma_{ff} = \sigma_f \left[1 + \frac{3\left(\frac{\sigma_s}{\sigma_f} - 1\right)\phi}{\left(\frac{\sigma_s}{\sigma_f} + 2\right) - \left(\frac{\sigma_s}{\sigma_f} - 1\right)\phi} \right] \quad (5)$$

As for the Newtonian fluid [46] defines the effective dynamic viscosity μ_{ff} of the ferrofluid and extends it to

$$\mu_{ff} = \frac{\mu_f}{(1-\phi)^{2.5}} \quad (6)$$

Considering the preceding attributes, the thermal diffusivity (α_{ff}) [47] is given as:

$$\alpha_{ff} = \frac{k_{ff}}{(\rho C_\rho)_{ff}} \quad (7)$$

2.2. Governing Dimensional Equations

An incompressible, electrically conducting ferrofluid in two dimensions that follows the basic Boussinesq approximation around a sphere with no temperature change with a radius submerged in a permeable substance is taken into consideration. The circle in the center represents a sphere of radius "a". This sphere is the object from which heat is being transferred due to convection. The green elliptical shapes surrounding the sphere represent the saturated permeable (porous) medium. This medium is likely a solid with interspersed voids or channels through which the ferrofluid can flow. The voids are where the ferrofluid flows and heat transfer occurs between the sphere and the fluid moving through these voids. We refer to this flow as a boundary-layer flow of two dimensions, laminar free convection. Analysis of non-Darcy flow can be done using an adaptation of the Forchheimer equation, which characterizes fluid flow while taking an inertial effect into account. Specifically, the coefficient that is not Darcy in the formula, which is an empirical number based on the fluid characteristics and pore geometry, denotes inertial resistance in a permeable media [48]. Both the base fluid and the rigid ferro-particles are thought to be in thermal balance and to be flowing at the same speed. When a consistent transverse magnetic field of intensity B_0 is present, the fluid temperature in the surrounding air is taken to be T_∞.

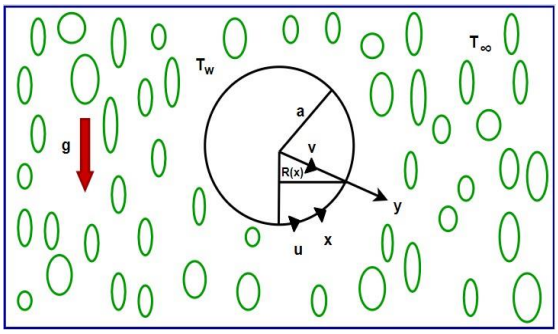

Fig. 1. Free convection on a sphere in a saturated permeable medium

The surface temperature of the sphere is thought to be T_w, where $T_w > T_\infty$ [49] which indicates that the sphere is at a higher temperature than its surroundings. Both the physical model and the coordinate system are shown in Figure 1 [50]. The coordinates x and y are used to estimate the distances between the stagnation point and the sphere's surface as well as the distance normal to it. The radius of the sphere(r) is marked, showing the distance from the center of the sphere to its surface. The downward arrow labeled as **g** indicates the direction of gravity**.** In free convection, gravity plays a crucial role as it causes the heated fluid (ferrofluid in this case) near the sphere to rise due to buoyancy while cooler fluid moves downwards. The variable**s** u and v denote the velocity components of the fluid in the x and y directions, respectively. These velocity fields are important for analyzing how the fluid moves around the sphere and within the porous medium.

The governing equations in dimensional form for mass continuity, momentum, and energy have the following forms under the Boussinesq and boundary layer approximations [49]:

- Continuity Equation:

$$\frac{\partial}{\partial \breve{x}}(\breve{r}\ \breve{u}) + \frac{\partial}{\partial \breve{y}}(\breve{r}\ \breve{v}) = 0 \quad (8)$$

- Momentum Equation:

$$\rho_{ff}\left(\frac{\breve{u}}{\in}\frac{\partial \breve{u}}{\partial \breve{x}} + \frac{\breve{v}}{\in}\frac{\partial \breve{u}}{\partial \breve{y}}\right) = \mu_{ff}\frac{\partial^2 \breve{u}}{\partial \breve{y}^2} - \sigma_{ff} B_0{}^2 \breve{u} - \frac{\in \mu_{ff}}{K}\breve{u} - \frac{1.75\rho_{ff}}{\sqrt{150 \in K}}\breve{u}^2 + g(\rho\beta)_{ff}(T - T_\infty)\sin\left(\frac{\breve{x}}{a}\right) \quad (9)$$

- Energy Equation:

$$\breve{u}\frac{\partial T}{\partial \breve{x}}+\breve{v}\frac{\partial T}{\partial \breve{y}}=\frac{k_{ff}}{\left(\rho C_p\right)_{ff}}\frac{\partial^2 T}{\partial \breve{y}^2} \tag{10}$$

where, $\breve{r}\left(\breve{x}\right)=a\sin\left(\breve{x}/a\right)$ [49] is the radial distance, K is the permeability of porous media, and ϵ is porosity parameter.

The following are the boundary conditions for the present problem:

$$\begin{aligned}&\breve{u}=0,\ \breve{v}=0,\ T=T_w \ \text{ at } \breve{y}=0\\&\breve{u}\to 0,\ T\to T_\infty \ \text{ as } \breve{y}\to\infty\end{aligned} \tag{11}$$

which means at $\breve{y}=0$ (the surface of the sphere): $\breve{u}=0,\ \breve{v}=0,$ This indicates that there is no fluid motion (both the tangential and radial velocity components are zero), which suggests that the sphere's surface is non-slip.

- $T=T_w$: The sphere's surface is kept at a constant temperature since the temperature there is equal to the wall temperature, T_w.

As $\breve{y}\to\infty$ (far from the sphere): $\breve{u}\to 0$: There is no disturbance in the fluid velocity field far from the sphere, as indicated by the velocity tending to zero.

- $T\to T_\infty$: The temperature distant from the sphere T_∞, which stands for the fluid's ambient temperature far from the sphere's surface

The transformation which is used for non-dimensionalization is as follows [49, 51]:

$$\begin{aligned}&x=\frac{\breve{x}}{a},\ y=Gr^{\frac{1}{4}}\frac{\breve{y}}{a},\ u=\frac{a}{\upsilon_f}Gr^{\frac{-1}{2}}\breve{u}\\&v=\frac{a}{\upsilon_f}Gr^{\frac{-1}{4}}\breve{v},\ \theta=\frac{A}{B}\\&Gr=\frac{g\beta_f\left(B\right)a^3}{\upsilon_f^2}\end{aligned} \tag{12}$$

where $A=(T-T_\infty)$, $B=(T_w-T_\infty)$, $\nu_f\left(=\mu_f/\rho_f\right)$ is the kinematic viscosity, Gr is the Grashof number, β_f is the volumetric coefficient of thermal expan- sion of the fluid and θ is the dimensionl- ess temperature. Thus, we have

$$r\left(x\right)=a\sin x \tag{13}$$

Equations (14), (15), and (16) provide the translated dimensionless equations:

$$\frac{\partial}{\partial x}\left(ru\right)+\frac{\partial}{\partial y}\left(rv\right)=0 \tag{14}$$

$$\begin{aligned}\frac{u}{\epsilon}\frac{\partial u}{\partial x}+\frac{v}{\epsilon}\frac{\partial u}{\partial y}=&\frac{\mu_{ff}\,\rho_f}{\mu_f\,\rho_{ff}}\frac{\partial^2 u}{\partial y^2}-\frac{\rho_f Ha^2 u}{\rho_{ff}Gr^{\frac{1}{2}}}\\&-\frac{\mu_{ff}\,\rho_f}{\mu_f\,\rho_{ff}}\frac{\epsilon u}{DaGr^{\frac{1}{2}}}-\frac{1.75u^2}{\sqrt{150\epsilon Da}}\\&+\theta\sin x\,\frac{(\rho\beta)_{ff}}{\rho_{ff}\,\beta_f}\end{aligned} \tag{15}$$

$$u\frac{\partial\theta}{\partial x}+v\frac{\partial\theta}{\partial y}=\frac{1}{\Pr}\frac{\alpha_{ff}}{\alpha_f}\frac{\partial^2\theta}{\partial y^2} \tag{16}$$

The following is the format of the boundary conditions (12):

$$\begin{aligned}&u=0,\ v=0,\ \theta=1 \ \text{ at } y=0\\&u\to 0,\ \theta\to 0 \ \text{ as } y\to\infty\end{aligned} \tag{17}$$

where, $\Pr\,(=\nu_f/\alpha_f)$ is the Prandtl num- ber, $Da(=K/a^2)$ is the Darcy number, and $Ha\left(=B_0 a\sqrt{\sigma_f/\mu_f}\right)$ is the Hartmann number,

3. Parabolic Transformation

The transformation is,

$$\begin{aligned}&X=x,\ Y=y,\ V=v,\ \Theta=\theta\\&R=a\sin X,\ U=\frac{u}{x}\end{aligned} \tag{18}$$

The parabolic transformed equations are given in Equations (19), (20), and (21):

$$X\frac{\partial U}{\partial X}+\left(1+X\frac{\cos X}{\sin X}\right)U+\frac{\partial V}{\partial Y}=0 \tag{19}$$

$$\begin{aligned}\frac{U^2}{\epsilon}+\frac{UX}{\epsilon}\frac{\partial U}{\partial X}+\frac{V}{\epsilon}\frac{\partial u}{\partial y}=&\frac{\mu_{ff}\,\rho_f}{\mu_f\,\rho_{ff}}\frac{\partial^2 U}{\partial Y^2}\\&-\frac{\rho_f Ha^2 U}{\rho_{ff}Gr^{\frac{1}{2}}}-\frac{\mu_{ff}\,\rho_f}{\mu_f\,\rho_{ff}}\frac{\epsilon U}{DaGr^{\frac{1}{2}}}\\&-\frac{1.75U^2X}{\sqrt{150\epsilon Da}}+\theta\frac{\sin X}{X}\frac{(\rho\beta)_{ff}}{\rho_{ff}\,\beta_f}\end{aligned} \tag{20}$$

$$XU\frac{\partial\Theta}{\partial X}+V\frac{\partial\Theta}{\partial Y}=\frac{1}{\Pr}\frac{\alpha_{ff}}{\alpha_f}\frac{\partial^2\Theta}{\partial Y^2} \tag{21}$$

Accordingly, boundary conditions are:

$$\begin{aligned}&U=0,\ \mathrm{V}=0,\ \Theta=1 \ \text{ at } \mathrm{Y}=0\\&U\to 0,\ \Theta\to 0 \ \text{ as } \mathrm{Y}\to\infty\end{aligned} \tag{22}$$

4. Numerical Procedure

FDM is used to solve the governing equation (19–21) of the sphere and the accompanying boundary conditions (22). The central difference discredits the diffusion terms in the momentum, continuity, and energy equations. For the convection terms, a forward difference scheme is also used. The Gaussian elimination approach is used to solve the resulting system of the equations. The program code of this method was developed in FORTRAN 90. In computat ion, we start with the energy equation to determine θ and then use the momentum equation to calculate tangential velocity U Lastly, the continuity equation is solved for normal velocity V directly. Beginning at X=0.0, the computation proceeds implicitly downstream. Here, the x and y grids are represented by the values Δx=0.02 and Δy = 0.01 correspondingly.

The physical quantities of primary importance in practical applications are the shearing stress and the heat transfer rate, expressed in terms of the Nusselt number Nu, and the skin-friction coefficient C_f respectively, which can be written as [51]:

$$C_f = \frac{\tau_w}{\rho_f U_\infty^2} \quad \text{and} \quad Nu = \frac{aq_w}{k_f (T_w - T_\infty)} \tag{23}$$

where

$$\tau_w = \mu_{ff} \left(\frac{\partial \breve{u}}{\partial \breve{y}} \right)_{\breve{y}=0} \quad \text{and} \quad q_w = -k_{ff} \left(\frac{\partial T}{\partial \breve{y}} \right)_{\breve{y}=0}$$

According to the following dimensionless relations, we are able to measure the physical quantity, the rate of heat transfer, which is significant from an application standpoint:

$$C_f Gr^{\frac{1}{4}} = X \left(\frac{\partial U}{\partial Y} \right)_{Y=0} \tag{24}$$

$$NuGr^{-\frac{1}{4}} = \frac{k_{ff}}{k_f} \left(\frac{\partial \theta}{\partial Y} \right)_{Y=0} \tag{25}$$

4.1. Code Validation

Several writers have determined the rate of heat transfer Nu in the absence of a magnetic field using equation (25). We have compared the quantitative behavior of the local Nusselt number with the research of Huang and Chen [52] and Nazar et al. [53] in order to validate the code for MHD natural flow. Here, Prandtl numbers $Pr = 7.0$ and $Pr = 0.7$ are selected, and the ferroparticle effect parameter and magnetic effect parameter have been disregarded. The flow pattern of the current investigation accords with the published result, according to Table 3, which compares the current numerical outcomes of the local Nusselt number with the results obtained by [52] and [53].

Table 3. Comparisons the current numerical results of local Nu with those obtained by Huang and Chen [52] and Nazar et al. [53] for the Prandtl numbers $Pr = 7.0$ and $Pr = 0.7$ without the effect of the volume fraction parameter and Hartmann number

	$Pr = 7.0$		
X in degree	Huang &Chen [52]	Nazar etal. [53]	Present results
0	0.9581	0.9595	0.9582
10	0.9559	0.9572	0.9570
20	0.9496	0.9506	0.9504
30	0.9389	0.9397	0.9399
40	0.9239	0.9239	0.9248
50	0.9045	0.9045	0.9057
60	0.8805	0.8801	0.8822
70	0.8518	0.8510	0.8535
80	0.8182	0.8168	0.8197
90	0.7792	0.7774	0.7808
	$Pr = 0.7$		
X in degree	Huang & Chen [52]	Nazar etal. [53]	Present results
0	0.4574	0.4576	0.4576
10	0.4563	0.4565	0.4566
20	0.4532	0.4533	0.4537
30	0.4480	0.4480	0.4484
40	0.4407	0.4405	0.4411
50	0.4312	0.4308	0.4317
60	0.4194	0.4189	0.4199
70	0.4053	0.4046	0.4059
80	0.3886	0.3879	0.3892
90	0.3694	0.3684	0.3698

From Table 3 it is clear that our result agrees with the previously published result in a good manner.

5. Results and Discussion

The focus of this work is on how the magnetic field affects the free convection flow of ferrofluid across an isothermal sphere submerged in permeable media, as measured by the Hartmann number (Ha), the volume fraction coefficient of ferroparticle ϕ and the porosity parameter (ϵ). Here, the Finite Difference Method (FDM), a very effective technique, is used to acquire numerical results. Tecplot, a visualizing program, is used to provide a graphic representation of the results.

The quantitative results are obtained for representative values of the volume frac- tion coefficient of ferrofluid (ϕ = 0%, 2%, 4%, 6%). Hartmann number $Ha(= 0.0, 1.0, 3.0, 5.0)$ and porosity parameter $\epsilon(= 0.4, 0.6, 0.8)$ while Prandtl number $Pr = 6.8733$, Grashof number $Gr = 1$ and Darcy number $Da = 10^{-2}$. Finally, the impact of Hartmann number (Ha), volume fraction coefficient of ferrofluid ϕ, and porosity parameter ϵ are shown on velocity and temperature distributions, local Nusselt number, and skin friction coefficient throughout the analysis. Moreover, streamlines and isotherms are also drawn to analyze the flow pattern.

5.1. Effect of Hartmann Number (Ha)

The ratio of the electrical force to the viscous force is known as the Hartmann number (Ha). It frequently happens when liquids move through magnetic fields.

To illustrate how the Hartmann number (Ha) affects things, the values of volume fraction (ϕ = 0%, 2%, 4%, 6%). and porosity parameter ($\epsilon = 0.4$) are considered fixed. Here, $Ha = 0.0$ stands for no magnetic effect. The value of Ha is moderately increased and detects the effect on velocity and temperature profiles as well as on skin friction coefficients, local Nusselt number, streamlines, and Isotherms.

The temperature and velocity curves for several Hartmann number ($Ha = 0.0, 1.0, 3.0, 5.0$) combinations are shown in Figure 2 with volume fraction coefficient $\phi = 2\%$, whereas the porosity parameter $\epsilon = 0.4$. Figure 2 makes it abundantly evident that when the Hartmann number (Ha) increases, the velocity distribution diminishes. The scenario in which there is no magnetic field is introduced by $Ha = 0$. When an electrically conducting flow is introduced into an electromagnetic field, the Lorentz force is generated. As the strength of the magnetic field rises, the Lorentz force also rises. Which causes the fluid velocity to decrease.

As a result, the velocity rapidly declines to zero in the free stream after reaching its peak at the sphere's surface. The electrically non-conducting situation ($Ha = 0$) is obviously the maximum velocity. In other words, it could be said that higher values of Ha the magnetic field slows the fluid flow, and conduction becomes the dominant mode of heat transfer. Conversely, as the figures illustrate, the fluid temperature rises as Ha does. In actuality, as the magnetized field intensity increases, the fluid loses further energy, resulting in a rise in thermal energy and an increase in temperature. Joule heating provides physical justification for this finding. The temperature steadily drops to zero in the free stream after reaching its maximum at the wall.

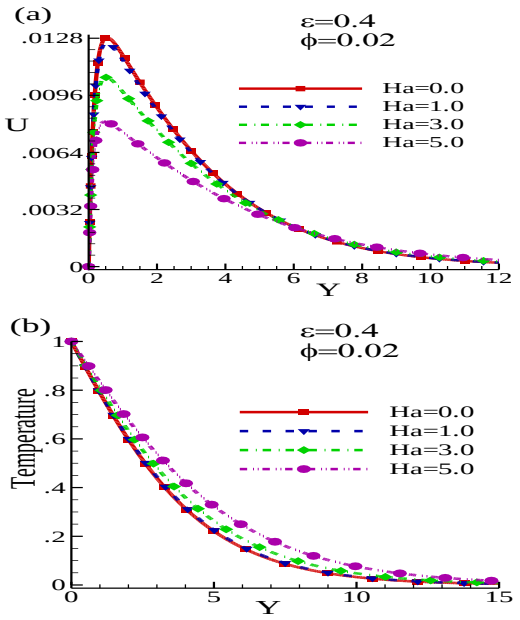

Fig. 2. (a) Velocity outlines with $\epsilon = 0.4$ and $\phi = 0.02$ for different values of Ha; (b) Temperature outlines with varying Ha values at $\phi = 0.02$ and $\epsilon = 0.4$

Figure 3 shows how the C_f and N_u with volume fraction $\phi = 2\%$ for porosity $\epsilon = 0.4$ are affected by variations in the Hartmann number ($Ha = 0.0, 1.0, 3.0, 5.0$). Figure 3 clearly shows that the skin friction coefficients and the local Nusselt number fall in tandem with an increase in the Hartmann number Ha. It is clear that C_f rises when the field of magnets is absent (Ha = 0.0) and falls when the field of magnets increases. This is mostly because rises in Ha affects the amplification of the Lorentz force, which lowers the momentum of the boundary layer. Decreasing surface shear stress and slowing down ferrofluid flow lowers the C_f and the Nusselt number.

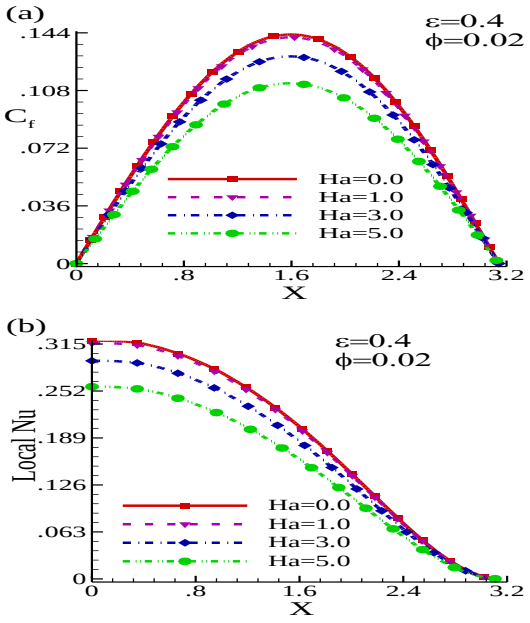

Fig. 3. (a) Skin friction coefficients profiles with $\epsilon = 0.4$ and $\phi = 0.02$ for different values of Ha; (b) Local Nusselt number with varying Ha values at $\phi = 0.02$ and $\epsilon = 0.4$

The effects of $Ha\ (=0.0, 1.0, 3.0, 5.0)$ with $\phi = 2\%$ and porosity $\epsilon = 0.4$ on isotherms and streamlines are shown in Figures 4 and 5. In Figure 4, When $Ha = 0.0$, this case represents no magnetic field. The streamlines are symmetric, showing a natural fluid flow pattern without external forces disrupting it. The flow appears smooth, with streamlines curving gently near the boundaries, indicating a typical fluid behavior in the absence of a magnetic field. $Ha = 1.0$, a moderate magnetic field is introduced. The streamlines are slightly more compact and begin to show some distortion compared to the $Ha = 0$ case. The magnetic field is now influencing the flow, leading to a more pronounced curvature of the streamlines near certain regions. As Ha increases to 3.0, the magnetic field's effect becomes stronger. The streamlines show significant distortion, indicating that the magnetic field is affecting the flow more prominently. The flow structure is more confined, and streamlines are packed more closely in some areas, suggesting stronger interactions between the magnetic field and the fluid. With $Ha = 5.0$, representing an even stronger magnetic field, the streamlines show maximum distortion. The flow pattern is heavily influenced by the magnetic field, with streamlines being tightly packed and curved in certain regions, indicating that the fluid movement is more constrained and affected by the Lorentz force induced by the magnetic field.

In Figure 5, when $Ha = 0.0$, isotherms are more evenly spaced, indicating a relatively natural and smooth heat transfer. The curvature of the isotherms suggests a natural temperature gradient where the heat diffuses uniformly. With $Ha = 1.0$, the isotherms become more concentrated near the boundary regions, indicating a stronger temperature gradient near those regions. The magnetic field slightly constrains the heat flow, leading to more curved isotherms compared to the $Ha = 0.0$ case. For a stronger magnetic field $Ha = 3.0$, the isotherms are more tightly packed, especially near the boundaries and the center. This indicates a steeper temperature gradient, meaning the magnetic field is increasingly affecting the thermal distribution. The flow of heat is more confined and directed, likely due to the interaction between the magnetic field and the fluid, which influences thermal diffusion. At $Ha = 5.0$, the strongest magnetic field, in this case, the isotherms are even more tightly packed and highly curved. This suggests that the magnetic field strongly influences how heat is distributed, causing heat to become more confined and the temperature gradients to increase. The tight clustering of isotherms near certain regions indicates a much higher rate of heat transfer in localized areas.

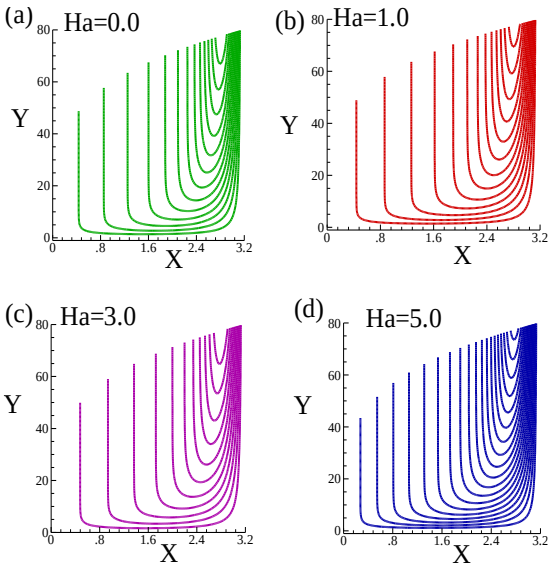

Fig. 4. Stream Lines for various values of Ha while $\epsilon = 0.4$ and $\phi = 0.02$

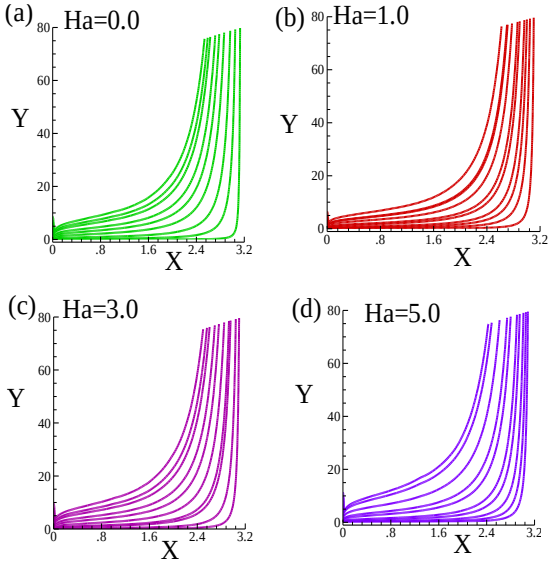

Fig. 5. Isotherms for various values of Ha while $\epsilon = 0.4$ and $\phi = 0.02$.

5.2. *Effect of Ferroparticle Volume Fractions* (ϕ)

Observing how volume fraction coefficients (ϕ) of ferroparticles are affected, the values of Hartmann number $Ha(= 0.0,\ 1.0, 3.0, 5.0)$ and $\epsilon(= 0.4)$ have remained fixed.

Figure 6 illustrates the velocity profiles with various combinations of volume fractions for the Hartmann number $Ha(= 0.0, 1.0, 3.0, 5.0)$ and porosity $\epsilon = 0.4$. It depicts that the velocitydecreases due to the increment in volume fractions. Physical justification for this can be found in the fact that a higher ferroparticle volume percentage raises the ferrofluid's thermal conductivity, which causes the thermal boundary layer's thickness and viscosity to rise and velocity to fall. When $\phi = 0\%$, it represents that there is no effect

of ferrofluid. It is prominent that up to a certain period, the effect of volume fraction is negligible, but afterthat, the velocity decreases significantly with the increasing value of volume fractions (ϕ).

Figure 7 demonstrates the temperature profile with various combinations of volume fraction coefficients for $Ha(= 0.0, 1.0, 3.0, 5.0)$ and $\epsilon = 0.4$. From Figure 7 it isseen that for the increasing value of ϕ coefficients, the variation in temperature profile is significant. We are also pragmatic from Figure 7 that the temperature is increased when the volume fraction parameters are increasing that is, if we upgrade the volume fraction, then the temperature will increase. Since thermal conductivity increases due to an increase of ϕ, so the temperature is increased.

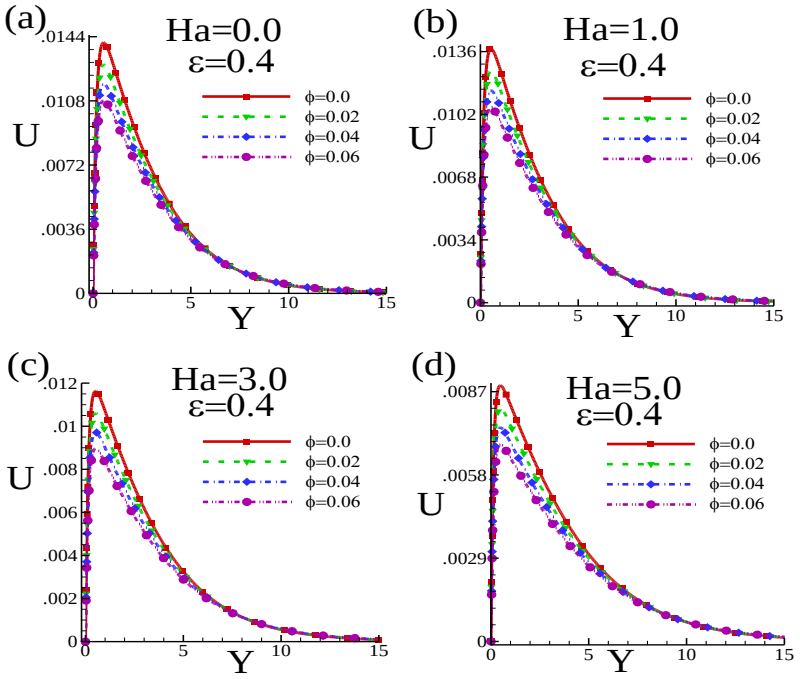

Fig. 6. (a) Velocity outlines for different ϕ when $\epsilon = 0.4$ and $Ha = 0.0$, (b) Velocity outlines for different ϕ when $\epsilon = 0.4$ and $Ha = 1.0$, The following are the velocity outlines: (c) For different ϕ when $\epsilon = 0.4$ and $Ha = 3.0$, and (d) For different ϕ when $\epsilon = 0.4$ and $Ha = 5.0$.

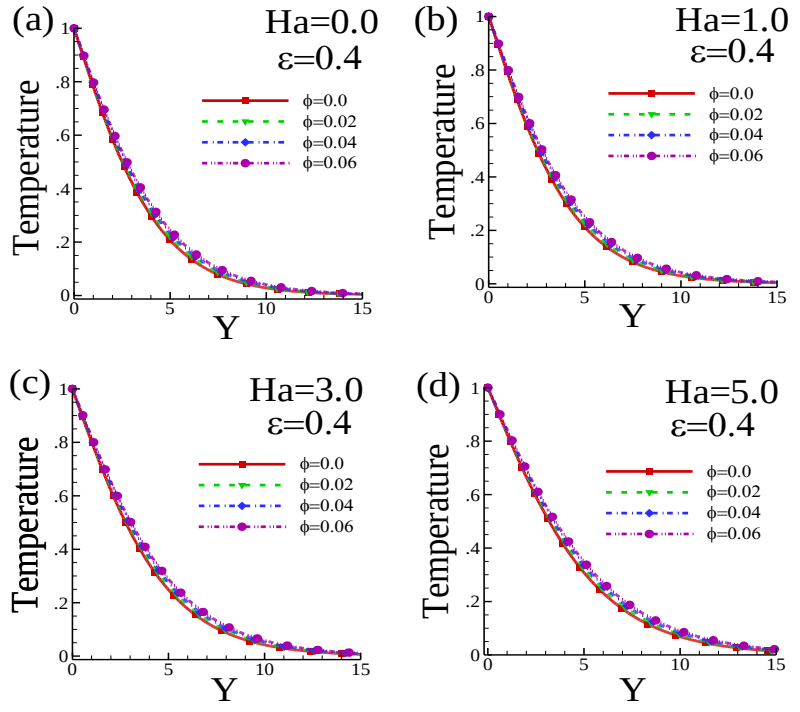

Fig. 7. (a) Temperature outlines for different ϕ when $\epsilon = 0.4$ and $Ha = 0.0$, (b) Temperature outlines for different ϕ when $\epsilon = 0.4$ and $Ha = 1.0$, The following are the temperature outlines: (c) For different ϕ when $\epsilon = 0.4$ and $Ha = 3.0$, and (d) For different ϕ when $\epsilon = 0.4$ and $Ha = 5.0$.

Figures 8 and 9 demonstrate the effect of the ϕ on the C_f profile and local Nu for various values of (ϕ = 0%, 2%, 4%, 6%) with $Ha(= 0.0, 1.0, 3.0, 5.0)$ and $\epsilon = 0.4$. It is evident from figures 8 and 9 that rises in the volume fraction coefficient results in a fall in both the skin friction coefficient and the local N_u. In terms of performance, fluid viscosity appeared to be enhanced by the ferroparticles volume fraction. Therefore, this observation implies that increased ferroparticle volume fraction can lower surface shear stress, which in turn lowers skin friction and local Nu. This, in turn, produces a significant increase in heat transfer; that is, if we increase volume fraction, then local Nu and skin friction coefficient will decrease.

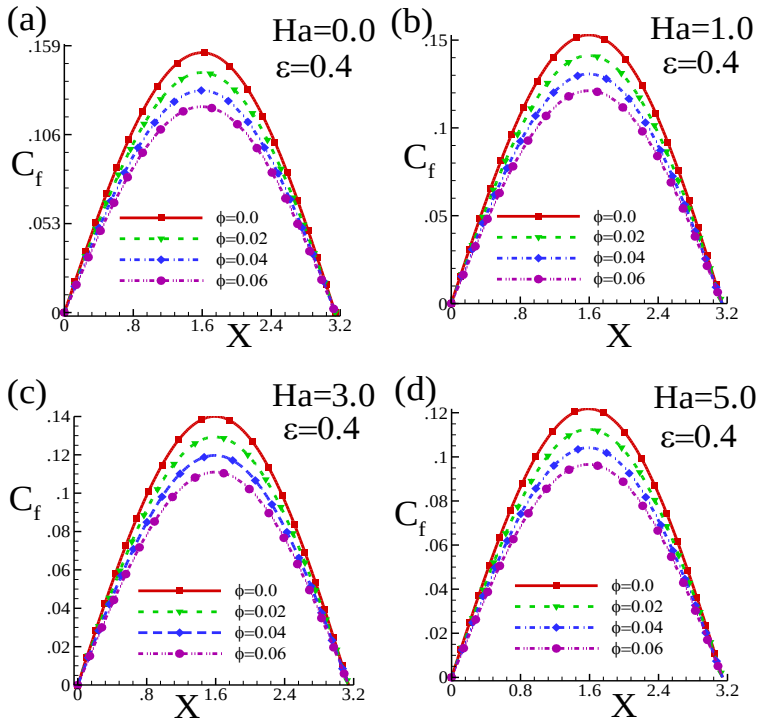

Fig. 8. (a) Skin friction coefficients for various ϕ values when $\epsilon = 0.4$ and $Ha = 0.0$, (b) Skin friction coefficients profiles for various ϕ values when $\epsilon = 0.4$ and $Ha = 1.0$, The following are the Skin friction coefficients profiles: (c) For various values of ϕ when $\epsilon = 0.4$ and $Ha = 3.0$, and (d) For various values of ϕ when $\epsilon = 0.4$ and $Ha = 5.0$.

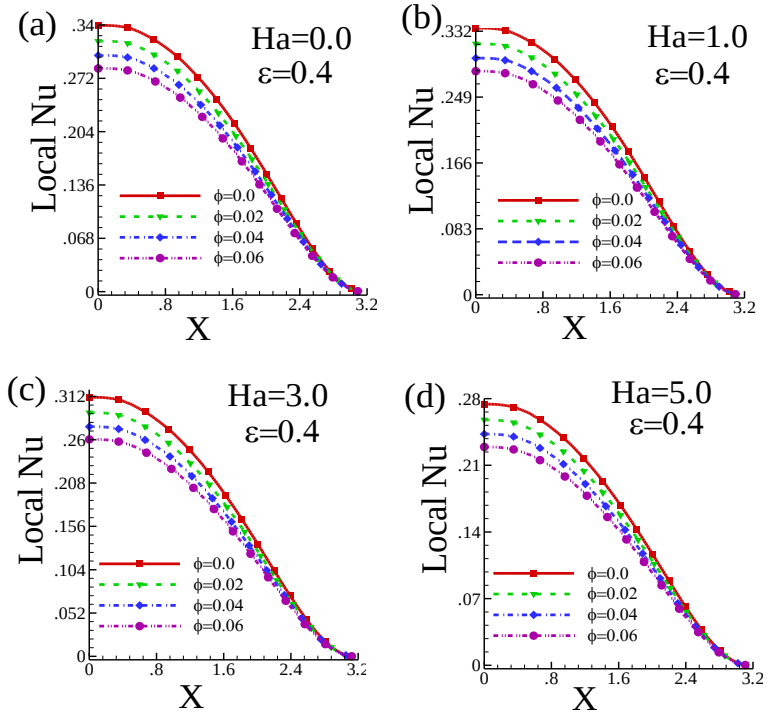

Fig. 9. (a) Local N_u for different ϕ when $\epsilon = 0.4$ and $Ha = 0.0$, (b) Local N_u for different ϕ when $\epsilon = 0.4$ and $Ha = 1.0$, The following are the Local N_u outlines: (c) For different ϕ when $\epsilon = 0.4$ and $Ha = 3.0$, and (d) For different ϕ when $\epsilon = 0.4$ and $Ha = 5.0$.

5.3. Effect of Porosity Parameter (ϵ)

A crucial factor in characterizing the internal structure of materials is porosity. Related to the overall volume of the material, it represents the volume of intersections that may hold fluid. In order to observe how the porosity parameter ($\epsilon = 0.4, 0.6, 0.8$) of ferroparticles works, the values of Hartmann number $Ha(= 1.0)$ and volume fraction $\phi(= 2\%)$ are remained fixed.

Figure 10 illustrates the impact of ϵ on temperature and velocity. The velocity distribution obviously reduces as the porosity parameter increases, but the temperature distribution grows as the porosity parameter rises. Since the Darcian body force is inversely proportional to permeability of the medium, so it decelerates the fluid flow in the boundary layer region and the opposite phenomena is observed for temperature profile.

Figure 11 makes it evident that when the porosity parameter ϵ increases, the C_f and N_u both fall down. Thus, the local N_u outlines and C_f outlines are highly dependent on the porosity parameter. This is because the porous material contributes positively to the increase in conduction on the heat transfer mode and as a consequence the Nusselt number increased by reduction of porosity.

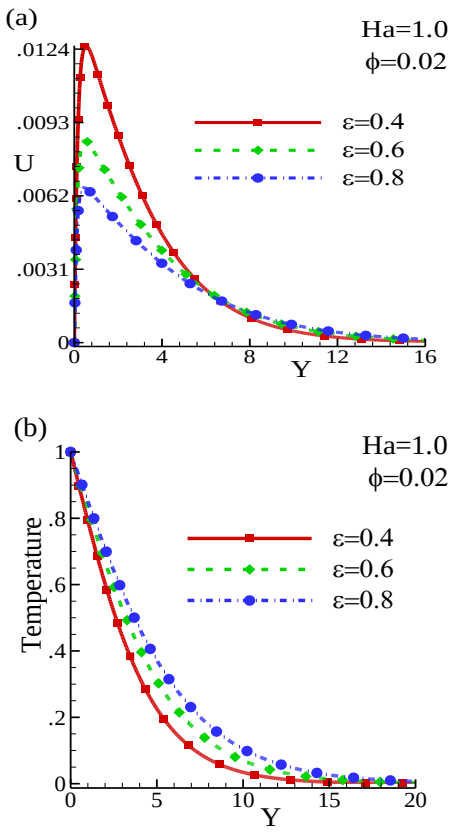

Fig. 10. (a) Velocity outlines with $Ha = 1.0$ and $\phi = 0.02$ for different ϵ (b) Temperature outlines with varying ϵ at $\phi = 0.02$ and $Ha = 1.0$

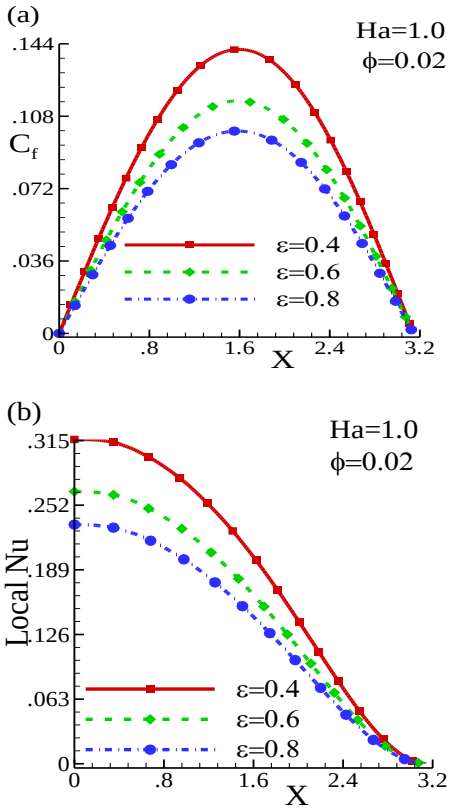

Fig. 11. (a) Distribution of the skin friction for different ϵ when $Ha = 1.0$ and $\phi = 0.02$, (b) The local Nusselt number for different ϵ values with $\phi = 0.02$ and $Ha = 1.0$

Figures 12 demonstrate how much the porosity parameter ϵ influences the growth of streamlines. The streamlines' spacing and curvature alter as ϵ varies, revealing how the fluid flow reacts to this parameter shift. For $\epsilon = 0.4$, the streamlines are relatively spread out, suggesting a more uniform or less obstructed flow. When $\epsilon = 0.6$, the streamlines show a more noticeable curvature, possibly indicating an increased interaction or influence of some internal force (perhaps magnetic or viscous effects), and lastly $\epsilon = 0.8$, the streamlines appear to be even more closely packed or curved, suggesting the strongest deviation or interaction with the force field or geometry.

Figure 13 demonstrates when ϵ changes, the shape and spacing of the isotherms are altered, indicating how thermal behavior changes with this parameter. For $\epsilon = 0.4$, the isotherms are more closely spaced near the boundary and spread out in the upper region. This suggests a steeper temperature gradient near the bottom and a more gradual distribution as you move upward. When $\epsilon = 0.6$, the isotherms appear more curved and concentrated near the central region. This indicates a stronger temperature gradient in the middle portion of the domain, and lastly for $\epsilon = 0.8$, the isotherms are even more tightly packed near the central and upper parts of the figure. This suggests the highest temperature gradient, with heat being more confined to certain regions.

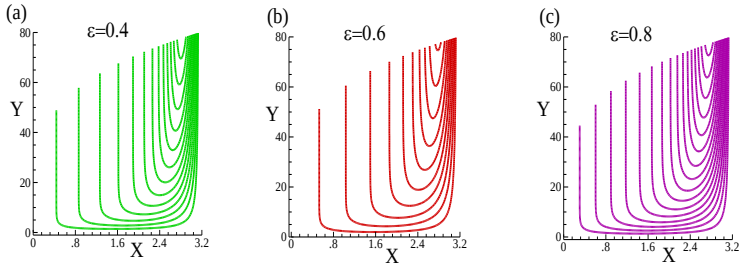

Fig. 12. Stream lines with various ϵ values when $Ha = 1.0$ and $\phi = 0.02$

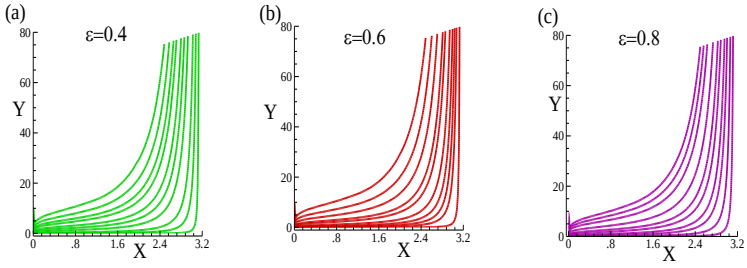

Fig. 13. Isotherms with various ϵ values when $Ha = 1.0$ and $\phi = 0.02$

6. Conclusions

The influence of magnetohydrodynamics free convection flow of ferrofluid across an isothermal sphere submerged in permeable media is investigated numerically in this work. Throughout our computation, $Pr = 6.8733$ is used as the assumed constant Prandtl number of the base fluid. Iron oxides Fe_2O_3 and Fe_3O_4 distributed in (H_2O), make up the ferrofluid that is utilized. The governing boundary layer equations of motion are transformed into a non dimensional form, leading to a nonlinear system of partial differential equations. This nonlinear system is numerically calculated using a special and efficient method known as the Finite Difference Method (FDM).

The study has been conducted by varying three parameters: the magnetic parameter or Hartmann number (Ha), porosity parameter (ϵ), and the Volume fraction of ferroparticles (ϕ). These parameters have been identified as crucial factors, and as a result, the impact of different combinations of these parameters on fluid flow has been thoroughly investigated. The results are shown graphically. Ferrofluids are essential for applications requiring precise thermal control, such as chemical reactors, medicinal devices, and electronics cooling, because changes in temperature and velocity profiles affect how heat is dispersed and transported in these fluids. In systems where ferrofluids flow through porous surfaces, control over these profiles can result in improved perfor mance and increased heat transfer efficiency. The resistance a fluid encounters along solid boundaries is related to the skin friction coefficient, which has a direct impact on the energy needed to keep the fluid flowing. Practically speaking, knowing how magnetic fields change skin friction can result in designs that are designed to use the least amount of energy possible. This is particularly useful for cooling systems and ferro-fluid-related industrial operations. In practical applications, controlling these flow patterns can help engineers design systems where ferrofluid movement is optimized for tasks such as targeted cooling or controlled material deposition. Theoretically, this adds depth to the study of magnetohydrodynamics (MHD), especially in the unique environment created by porous media. From a theoretical standpoint, studying isotherms aids in predicting how magnetic fields can be used to control thermal behavior in ferrofluids, contributing to advancements in thermal management technologies.

The current investigation allows for the following findings to be made:

1. Velocity changes remarkably when Ha increases. The velocity decreases with the increasing value of Hartmann number Ha. The temperature profiles are more sensitive. The temperature is increased with the increasing value of the Hartmann number Ha.
2. Along the surface, the skin friction coefficients fluctuate. Both the local N_u and C_f are growing lower with rising Ha values.
3. For increasing Ha, figure of streamlines seems to depict functions with more gradual changes and for isotherms, represents functions with sharper, exponential-like increases.
4. The velocity is decreasing signify- cantly with the increasing value of volume fractions (ϕ). The temperature profiles are increasing with the decreasing value of volume fractions (ϕ).

5. Both the local N_u and C_f are growing lower with rising ϕ values.
6. The temperature profile rises, and the C_f and local N_u drop when the porosity parameter ϵ increases.
7. The velocity patterns within the boundary layer considerably decrease as the porosity parameter ϵ rises.

The principles elucidated by the study could be applied in thermal energy storage systems, where ferrofluids serve as heat transfer fluids. By understanding how magnetic fields affect their thermal behavior, engineers can design more efficient storage systems that can rapidly charge and discharge energy. The research may inspire the development of new smart materials that respond dynamically to magnetic fields, enhancing their performance in applications such as robotics, where precise control over heat and fluid movement is necessary. The implications of this study can extend beyond traditional engineering fields, promoting interdisciplinary research that integrates fluid dynamics, materials science, and magnetic field applications, leading to innovations in various sectors. This research has some limitations, too. The type and characteristics of the porous medium, such as porosity and permeability, may greatly influence the heat transfer process. Our results may vary with other materials. The research may focus on a specific magnetic field strength or configura tion, which could limit the generalizability of the findings. Future studies could investigate a wider range of magnetic field conditions and orientations to fully understand their effects.

Funding Statement

The financing needed to complete this project was provided by Jagannath University Bangladesh, for which the first and second authors are grateful.

Conflicts of Interest

The author declares that there is no conflict of interest regarding the publication of this article.

References

[1] Jang, J., Lee, S.S., 2000. Theoretical and experimental study of mhd(magne-(hydrodynamic) micropump. *Sensors and Actuators A: Physical*, 80(1), pp. 84-89.

[2] Shakeri, F., Dehghan, M., 2011. A finite volume spectral element method for solving magnetohydrodynamic (mhd) equations. *Applied Numerical Mathematics*, 61(1), pp. 1–23.

[3] Dehghan, M., Mirzaei, D., 2009. Meshless local petrovgalerkin (mlpg) method for the unsteady magnetohydro- dynamic (mhd) flow through pipe with arbitrary wall conductivity. *Applied Numerical Mathematics*, 59(5), pp. 1043-1058.

[4] Dehghan, M., Mirzaei, D., 2009. Meshless local boundary integral equation (lbie) method for the unsteady magnetohydrodynamic (mhd) flow in rectangular and circular pipes. *Computer Physics Communications*, 180(9) pp. 1458–1466.

[5] Sheikholeslami, M., Gorji-Bandpy, M., Ganji, D.D., 2014. Lattice boltzmann method for mhd natural convection heat transfer using nanofluid. *Powder Technology*, 254 pp. 82–93.

[6] Ellahi, R., 2013. The effects of mhd and temperature dependent viscosity on the flow of non-Newtonian nano- fluid in a pipe: analytical solutions. *Applied Mathematical Modelling*, 37(3), pp. 1451-1467

[7] Nakatsuka, K., Jeyadevan, B., Neveu, S., Koganezawa, H., 2002. The magnetic fluid for heat transfer applications. *Journal of Magnetism and Magnetic Materials*, 252 pp. 360–362.

[8] Poddar, S., Islam, M.M., Ferdouse, J., Alam, M.M., 2021. Characteristical analysis of mhd heat and mass transfer dissipative and radiating fluid flow with magnetic field induction and suction. *SN Applied Sciences*, 3, pp. 1–17.

[9] Ba¨ıri, A., Zarco-Pernia, E., De Mar´ıa, J.-M.G., 2014. A review on natural convection in enclosures for engi- neering applications. the particular case of the parallelogrammic diode cavity. *Applied Thermal Engineering*, 63(1), pp. 304–322.

[10] Ghandouri, I.E., Maakoul, A.E., Saadeddine, S., Meziane, M., 2023. A comprehensive review of methods used to improve the thermal per- formance of heat sinks in natural convection. *Heat and Mass Transfer*, 59(5), pp. 825–849.

[11] Henry, R., Tiselj, I., Matkovič, M. , 2017. Natural and mixed convection in the cylindrical pool of triga reactor. *Heat and Mass Transfer*, 53, pp. 537–551.

[12] Nikitin, E., Fridman, E., 2018. Extension of the reactor dynamics code dyn3d to sfr applications part iii: Valida- tion against the initial phase of the phenixeol natural convection test. *Annals of Nuclear Energy* 119, pp. 390–395.

[13] Ebrahimnia-Bajestan, E., Niazmand, H., Etminan-Farooji, V., Ebrahimnia, E., 2012, Numerical modeling of the freezing of a porous humid food inside a cavity due to natural convection. *Numerical Heat Transfer, Part A: Applications,* 62(3), pp. 250–269.

[14] Bhargava, N., Mor, R.S., Kumar, K., Sharanagat, V.S., 2021. Advances in application of ultrasound in food processing: A review. *Ultrasonics sonochemistry*, 70, pp. 105293.

[15] Sadeghi, M.S., Dogonchi, A., Ghodrat, M., Chamkha, A.J., Alhumade, H., Karimi, N., 2021. Natural convection of *CuO*-water nanofluid in a conventional oil/water sepa- rator cavity: Application to com- bined cycle power plants. *Journal of the Taiwan Institute of Chemical Engineers*, 124, pp. 307–319.

[16] Mohebbi, R., Mehryan, S., Izadi, M., Mahian, O., 2019. Natural convection of hybrid nanofluids inside a partitio- ned porous cavity for application in solar power plants. *Journal of Thermal Analysis and Calorimetry*, 137, pp. (2019) 1719–1733.

[17] Sekhar, B.C., Kumar, P.V., Veera Krishna, M., 2023. Changeable heat and mass transport on unsteady mhd convec- tive flow past an infinite vertical porous plate. *Journal of Heat and Mass Transfer Research*, 10(2), pp. 207–222.

[18] El Hamma, M., Aberdane, I., Taibi, M., Rtibi, A., Gueraoui, K., 2023. Analysis of mhd thermosolutal convection in a porous cylindrical cavity filled with a casson nanofluid, considering soret and dufour effects. *Journal of Heat and Mass Transfer Research*, 10(2), pp. 197–206.

[19] Ghasemi, B. Aminossadati, S., 2009. Natural convection heat transfer in an inclined enclosure filled with a water-cuo nanofluid. *Numerical Heat Transfer, Part A: Applications*, 55(8), pp. 807–823.

[20] Ragupathi, E., Prakash, D., Muthtamilselvan, M., Al-Mdallal, Q.M., 2024. A case study on heat transport of electrically conducting water based-cofe2o4 ferrofluid flow over the disc with various nanoparticle shapes and highly oscillating magnetic field. *Journal of Magnetism and Magnetic Materials*, 589, 171624.

[21] Rosensweig, R.E., 1982. *Magnetic fluids, Scientific American*, 247(4), pp. 136–145.

[22] Rosensweig, R.E., 1979. Fluid dynamics and science of magnetic liquids. *Advances in electronics and electron physics*, 48, pp. 103–199, Elsevier.

[23] Bailey, R., 1983. Lesser known applications of ferrofluids. *Journal of Magnetism and Magnetic Materials*, 39(1-2), pp. 178–182.

[24] Raj, K., Moskowitz, R., 1980. A review of damping applications of ferro- fluids. *IEEE Transactionson Magnetics*, 16(2), pp. 358–363.

[25] Raj, K., Moskowitz, R., 1990. Commercial applications of ferrofluids. *Journal of Magnetism and Magnetic Materials*, 85(1-3), pp. 233–245.

[26] Dong, Z.-Q., Li, X., Yamaguchi, H., Yu, P., 2024. Magnetic field effect on the sedimentation process of two non-magnetic particles inside a ferrofluid. *Journal of Magnetism and Magnetic Materials*, 589, (2024) 171501.

[27] Sheikholeslami, M., Rashidi, M., 2015. Ferrofluid heat transfer treatment in the presence of variable magnetic field. *The European Physical Journal Plus*, 130, pp. 1–12.

[28] Alsaady, M., Fu, R., Li, B., Boukhanouf, R., Yan, Y., 2015. Thermo-physical properties and thermo- magnetic convection of ferrofluid. *Applied Thermal Engineering*, 88, pp. 14–21.

[29] Farooq, U., Hassan, A., Fatima, N., Imran, M., Alqurashi, M., Noreen, S., Akgül, A., Bariq, A., 2023. A computatational fluid dynamics analysis on fe_3O_4–H_2O based nanofluid axisymmetric flow over a rotating disk with heat transfer enhance- ment. *Scientific Reports*, 13(1) 4679.

[30] Ghanbarian, B., Hunt, A.G., Ewing, R.P., Sahimi, M., 2013. Tortuosity in porous media: a critical review. *Soil Science Society of America Journal*, 77(5), pp. 1461–1477.

[31] Siddiqui, A.A., Turkyilmazoglu, M., 2020. Natural convection in the ferrofluid enclosed in a porous and permeable cavity. *International Communications in Heat and Mass Transfer*, 113, 104499.

[32] Sedghi-Asl, M., Afrasiabi, B., Rahimi, H., 2023. New correlations for non-darcy flow in porous media. *Acta Mechanica*, 234, pp. 4559–4572.

[33] Marafini, E., La Rocca, M., Fiori, A., Battiato, I., Prestininzi, P., 2020. Suitability of 2d modelling to evaluate flow properties in 3d porous media. *Transport in Porous Media*, 134, pp. 315–329.

[34] Song, Y.-Q., 2003. Using internal magnetic fields to obtain pore size distributions of porous media. *Concepts in Magnetic Resonance Part A: An Educational Journal*, 18(2), pp. 97–110.

[35] Sakthivel, S., Shukla, P., 2023. Drag on a porous sphere enclosed in a solid core embedded in couple stress fluid. *Special Topics & Reviews in Porous Media: An International Journal*, 14(1) pp. 61-78,

[36] B´eg, O.A., Zueco, J., Bhargava, R., Takhar, H.S., 2009. Magnetohydrodynamic convection flow from a sphere to a non-darcian porous medium with heat generation or absorption effects: network simulation. *International Journal of Thermal Sciences*, 48(5), pp. 913–921.

[37] Sivaraj, C., Sheremet, M., 2018. MHD natural convection and entropy generation of ferrofluids ina cavity with a non-uniformly heated horizontal plate. *International Journal of Mechanical Sciences*, 149, pp. 326–337.

[38] Dogonchi, A.S., Hashim, 2019. Heat transfer by natural convection of Fe_3O_4-water nanofluid in an annulus between a wavy circular cylinder and a rhombus. *International Journal of Heat and Mass Transfer*, 130, pp. 320–332.

[39] Shenoy, A., Sheremet, M., Pop, I., 2016. Convective flow and heat transfer from wavy surfaces: vis- cous fluids. *porous media, and nanofluids*, *CRC press*.

[40] Sheikholeslami, M., Rashidi, M.M., Ganji, D.D., 2015. Effect of non-uniform magnetic field on forced convectio- n heat transfer of Fe_3O_4–water nanofluid. *Computer Methods in Applied Mechanics and Engineering*, 294, pp. 299–312.

[41] Sheikholeslami, M., Rashidi, M.M., 2015. Effect of space dependent magnetic field on free convection of Fe_3O_4–water nanofluid. *Journal of the Taiwan Institute of Chemical Engineers*, 56, pp. 6–15

[42] Xuan, Y., Li, Q., 2000. Heat transfer enhancement of nanofluids. *International Journal of heat and fluid flow*, 21(1), 58–64.

[43] Ghanbarpour, M., Haghigi, E.B., Khodabandeh, R., 2014. Thermal properties and rheological behavior of water based al2o3 nanofluid as a heat transfer fluid. *Experimental Ther- mal and Fluid Science*, 53, pp. 227–235.

[44] Javed, T., Siddiqui, M.A., 2018. Effect of mhd on heat transfer through ferrofluid inside a square cavity containing obstacle/heat source. *International Journal of Thermal Sciences*, 125, 419–427.

[45] Sheremet, M.A., Oztop, H., Pop, I., Al-Salem, K., 2016. MHD free convection in a wavy open porous tall cavity filled with nanofluids under an effect of corner heater. *International Journal of Heat and Mass Transfer*, 103, pp. 955–964.

[46] Gangadhar, K., Vijayakumar, D., Chamkha, A.J., Kannan, T., Sakthivel, G., 2020. Effects of Newtonian heating and thermal radiation on micropolar ferrofluid flow past a stretching surface: spectral quasi-linearization method. *Heat Transfer*, 49(2), pp. 838-857.

[47] Ahmed, S., Hossain, A., Hossain, M.Z., Molla, M.M., 2023. Forced convection of non-Newtonian nanofluid in a sinusoidal wavy channel with response surface analysis and sensitivity test. *Results in Engineering*, 19, 101360.

[48] Elsanoose, A., Abobaker, E., Khan, F., Rahman, M.A., Aborig, A., Butt, S.D., 2022. Characterization of a non-darcy flow and development of new correlation of non-darcy coefficient. *Energies*, 15(20), 7616.

[49] Molla, M.M., Taher, M., Chowdhury, M.M., Hossain, M.A., 2005. Magnetohydrodynamic naturalconvection flow on a sphere in presence of heat generation. *Nonlinear Analysis: Modelling and Control*, 10(4), pp. 349–363.

[50] Moghimi, M., Talebizadeh, P., Mehrabian, M., 2011. Heat generation/absor- ption effects on magnetohydrodyn- amic natural convection flow over a sphere in a non-darcian porous medium.*Proceedings of the Institution of Mechanical Engineers, Part E: Journal of Process Mechanical Engineering*, 225(1), pp. 29–39.

[51] Molla, M.M., Hossain, M.A., Paul, M.C., 2006. Natural convection flow from an isothermal horizontal circular cylinder in presence of heat generation. *International Journal of Engineering Science*, 44(13-14), pp. 949–958.

[52] Huang, M., Chen, G., 1987. Laminar free convection from a sphere with blowing and suction. *Journal of Heat Transfer (Transactions of the ASME (American Society of Mechanical Engineers), Series C);(United States)*, 109(2), pp. 529–532.

[53] Nazar, R., Amin, N., 2002. Free convection boundary layer on an isothermal sphere in a micropolar fluid. *International communications in heat and mass transfer*, 29(3), pp. 377–386.